Biomedical Optics EXPRESS

Coherent anti-Stokes Raman scattering and spontaneous Raman spectroscopy and microscopy of microalgae with nitrogen depletion

X. N. He,[1] J. Allen,[2] P. N. Black,[2,5] T. Baldacchini,[1,3] X. Huang,[1] H. Huang,[1] L. Jiang,[4] and Y. F. Lu[1,*]

[1]*Department of Electrical Engineering, University of Nebraska-Lincoln, Lincoln, NE 68588-0511, USA*
[2]*Department of Biochemistry, University of Nebraska-Lincoln, Lincoln, NE 68588-0664, USA*
[3]*Technology and Applications Center, Newport Corporation, Irvine, CA 92606, USA*
[4]*Department of Mechanical and Automation Engineering, Beijing Institute of Technology, Beijing, 100081, China*
[5]*pblack2@unl.edu*
**ylu2@unl.edu*

Abstract: Microalgae are extensively researched as potential feedstocks for biofuel production. Energy-rich compounds in microalgae, such as lipids, require efficient characterization techniques to investigate the metabolic pathways and the environmental factors influencing their accumulation. The model green alga *Coccomyxa* accumulates significant amounts of triacylglycerols (TAGs) under nitrogen depletion (N-depletion). To monitor the growth of TAGs (lipid) in microalgal cells, a study of microalgal cells (*Coccomyxa* sp. C169) using both spontaneous Raman and coherent anti-Stokes Raman scattering (CARS) spectroscopy and microscopy were carried out. Spontaneous Raman spectroscopy was conducted to analyze the components in the algal cells, while CARS was carried out to monitor the distribution of lipid droplets in the cells. Raman signals of carotenoid are greater in control microalgae compared to N-depleted cells. Raman signals of lipid droplets appear after N-depletion and its distribution can be clearly observed in the CARS microscopy. Both spontaneous Raman spectroscopy and CARS microscopy were found to be suitable analysis tools for microalgae.

OCIS codes: (300.6365) Spectroscopy; (300.6230) Spectroscopy, coherent anti-Stokes Raman scattering; (300.6450) Spectroscopy, Raman.

References and links

1. Q. Hu, M. Sommerfeld, E. Jarvis, M. Ghirardi, M. Posewitz, M. Seibert, and A. Darzins, "Microalgal triacylglycerols as feedstocks for biofuel production: perspectives and advances," Plant J. **54**(4), 621–639 (2008).
2. S. A. Scott, M. P. Davey, J. S. Dennis, I. Horst, C. J. Howe, D. J. Lea-Smith, and A. G. Smith, "Biodiesel from algae: challenges and prospects," Curr. Opin. Biotechnol. **21**(3), 277–286 (2010).
3. R. H. Wijffels and M. J. Barbosa, "An outlook on microalgal biofuels," Science **329**(5993), 796–799 (2010).
4. L. Rodolfi, G. Chini Zittelli, N. Bassi, G. Padovani, N. Biondi, G. Bonini, and M. R. Tredici, "Microalgae for oil: strain selection, induction of lipid synthesis and outdoor mass cultivation in a low-cost photobioreactor," Biotechnol. Bioeng. **102**(1), 100–112 (2009).
5. J. Msanne, D. Xu, A. R. Konda, J. A. Casas-Mollano, T. Awada, E. B. Cahoon, and H. Cerutti, "Metabolic and gene expression changes triggered by nitrogen deprivation in the photoautotrophically grown microalgae *Chlamydomonas reinhardtii* and *Coccomyxa* sp. C-169," Phytochemistry **75**, 50–59 (2012).
6. A. Demirbas, "Importance of biodiesel as transportation fuel," Energy Policy **35**(9), 4661–4670 (2007).
7. R. J. Radmer and B. C. Parker, "Commercial applications of algae: opportunities and constraints," J. Appl. Phycol. **6**(2), 93–98 (1994).
8. J. Sheehan, T. Dunahay, R. Benemann, G. Roessler, and C. Weissman, "A look back at the U.S. department of energy's aquatic species program biodiesel from algae," National Renewable Energy Laboratory Report NREL/TP-580-24190 (July 1998).

#175376 - $15.00 USD Received 4 Sep 2012; revised 13 Oct 2012; accepted 15 Oct 2012; published 18 Oct 2012

9. G. A. Thompson, Jr., "Lipids and membrane function in green algae," Biochim. Biophys. Acta **1302**(1), 17–45 (1996).
10. H. J. van Manen, Y. M. Kraan, D. Roos, and C. Otto, "Single-cell Raman and fluorescence microscopy reveal the association of lipid bodies with phagosomes in leukocytes," Proc. Natl. Acad. Sci. U.S.A. **102**(29), 10159–10164 (2005).
11. C. L. Evans and X. S. Xie, "Coherent anti-stokes Raman scattering microscopy: chemical imaging for biology and medicine," Annu Rev Anal Chem (Palo Alto Calif) **1**(1), 883–909 (2008).
12. P. D. Maker and R. W. Terhune, "Study of optical effects due to an induced polarization third order in the electric field strength," Phys. Rev. **137**(3A), A801–A818 (1965).
13. J. X. Cheng and X. S. Xie, "Coherent anti-Stokes Raman scattering microscopy: Instrumentation, theory, and applications," J. Phys. Chem. B **108**(3), 827–840 (2004).
14. J. X. Cheng, Y. K. Jia, G. F. Zheng, and X. S. Xie, "Laser-scanning coherent anti-Stokes Raman scattering microscopy and applications to cell biology," Biophys. J. **83**(1), 502–509 (2002).
15. R. F. Begley, A. B. Harvey, and R. L. Byer, "Coherent anti-Stokes Raman spectroscopy," Appl. Phys. Lett. **25**(7), 387–390 (1974).
16. C. L. Evans, E. O. Potma, and X. S. Xie, "Coherent anti-stokes Raman scattering spectral interferometry: determination of the real and imaginary components of nonlinear susceptibility $\chi(3)$ for vibrational microscopy," Opt. Lett. **29**(24), 2923–2925 (2004).
17. E. O. Potma, C. L. Evans, and X. S. Xie, "Heterodyne coherent anti-Stokes Raman scattering (CARS) imaging," Opt. Lett. **31**(2), 241–243 (2006).
18. F. Ganikhanov, C. L. Evans, B. G. Saar, and X. S. Xie, "High-sensitivity vibrational imaging with frequency modulation coherent anti-Stokes Raman scattering (FM CARS) microscopy," Opt. Lett. **31**(12), 1872–1874 (2006).
19. A. Zumbusch, G. R. Holtom, and X. S. Xie, "Three-dimensional vibrational imaging by coherent anti-Stokes Raman scattering," Phys. Rev. Lett. **82**(20), 4142–4145 (1999).
20. M. Hashimoto, T. Araki, and S. Kawata, "Molecular vibration imaging in the fingerprint region by use of coherent anti-Stokes Raman scattering microscopy with a collinear configuration," Opt. Lett. **25**(24), 1768–1770 (2000).
21. C. L. Evans, E. O. Potma, M. Puoris'haag, D. Côté, C. P. Lin, and X. S. Xie, "Chemical imaging of tissue in vivo with video-rate coherent anti-Stokes Raman scattering microscopy," Proc. Natl. Acad. Sci. U.S.A. **102**(46), 16807–16812 (2005).
22. J. X. Cheng, Y. K. Jia, G. Zheng, and X. S. Xie, "Laser-scanning coherent anti-Stokes Raman scattering microscopy and applications to cell biology," Biophys. J. **83**(1), 502–509 (2002).
23. E. R. Dufresne, E. I. Corwin, N. A. Greenblatt, J. Ashmore, D. Y. Wang, A. D. Dinsmore, J. X. Cheng, X. S. Xie, J. W. Hutchinson, and D. A. Weitz, "Flow and fracture in drying nanoparticle suspensions," Phys. Rev. Lett. **91**(22), 224501 (2003).
24. G. W. H. Wurpel, J. M. Schins, and M. Müller, "Chemical specificity in three-dimensional imaging with multiplex coherent anti-Stokes Raman scattering microscopy," Opt. Lett. **27**(13), 1093–1095 (2002).
25. X. Nan, W. Y. Yang, and X. S. Xie, "CARS microscopy lights up lipids in living cells," Biophotonics Int. **11**, 44–47 (2004).
26. E. O. Potma and X. S. Xie, "Detection of single lipid bilayers with coherent anti-Stokes Raman scattering (CARS) microscopy," J. Raman Spectrosc. **34**(9), 642–650 (2003).
27. X. Nan, E. O. Potma, and X. S. Xie, "Nonperturbative chemical imaging of organelle transport in living cells with coherent anti-stokes Raman scattering microscopy," Biophys. J. **91**(2), 728–735 (2006).
28. J. H. Strickler and W. W. Webb, "Two-photon excitation in laser scanning fluorescence microscopy," Proc. SPIE **1398**, 107–118 (1991).
29. E. S. Wu, J. H. Strickler, W. R. Harrell, and W. W. Webb, "Two-photon lithography for microelectronic application," Proc. SPIE **1674**, 776–782 (1992).
30. T. Baldacchini, M. Zimmerley, C. H. Kuo, E. O. Potma, and R. Zadoyan, "Characterization of microstructures fabricated by two-photon polymerization using coherent anti-stokes Raman scattering microscopy," J. Phys. Chem. B **113**(38), 12663–12668 (2009).
31. K. Ikeda and K. Uosaki, "Coherent phonon dynamics in single-walled carbon nanotubes studied by time-frequency two-dimensional coherent anti-stokes Raman scattering spectroscopy," Nano Lett. **9**(4), 1378–1381 (2009).
32. S. A. Akhmanov, N. I. Koroteev, and A. I. Kholodnykh, "Excitation of the coherent optical phonons of E_g-type in calcite by means of the active spectroscopy method," J. Raman Spectrosc. **2**(3), 239–248 (1974).
33. D. Fu, F. K. Lu, X. Zhang, C. Freudiger, D. R. Pernik, G. Holtom, and X. S. Xie, "Quantitative chemical imaging with multiplex stimulated Raman scattering microscopy," J. Am. Chem. Soc. **134**(8), 3623–3626 (2012).
34. E. Ploetz, S. Laimgruber, S. Berner, W. Zinth, and P. Gilch, "Femtosecond stimulated Raman microscopy," Appl. Phys. B **87**(3), 389–393 (2007).
35. C. W. Freudiger, W. Min, B. G. Saar, S. Lu, G. R. Holtom, C. He, J. C. Tsai, J. X. Kang, and X. S. Xie, "Label-free biomedical imaging with high sensitivity by stimulated Raman scattering microscopy," Science **322**(5909), 1857–1861 (2008).

#175376 - $15.00 USD Received 4 Sep 2012; revised 13 Oct 2012; accepted 15 Oct 2012; published 18 Oct 2012

36. Y. Ozeki, Y. Kitagawa, K. Sumimura, N. Nishizawa, W. Umemura, S. i. Kajiyama, K. Fukui, and K. Itoh, "Stimulated Raman scattering microscope with shot noise limited sensitivity using subharmonically synchronized laser pulses," Opt. Express **18**(13), 13708–13719 (2010).
37. P. Nandakumar, A. Kovalev, A. Volkmer, "Vibrational imaging based on stimulated Raman scattering microscopy," New J. Phys. **11**, 033026 (2009).
38. B. G. Saar, C. W. Freudiger, J. Reichman, C. M. Stanley, G. R. Holtom, and X. S. Xie, "Video-rate molecular imaging in vivo with stimulated Raman scattering," Science **330**(6009), 1368–1370 (2010).
39. J. X. Cheng, A. Volkmer, L. D. Book, and X. S. Xie, "Multiplex coherent anti-Stokes Raman scattering microscopy and study of lipid vesicles," J. Phys. Chem. B **106**(34), 8493–8498 (2002).
40. J. X. Cheng, L. D. Book, and X. S. Xie, "Polarization coherent anti-Stokes Raman scattering microscopy," Opt. Lett. **26**(17), 1341–1343 (2001).
41. H. Kano and H. Hamaguchi, "Ultrabroadband (>2500 cm^{-1}) multiplex coherent anti-Stokes Raman scattering microspectroscopy using a supercontinuum generated from a photonic crystal fiber," Appl. Phys. Lett. **86**(12), 121113 (2005).
42. G. W. H. Wurpel, J. M. Schins, and M. Müller, "Chemical specificity in three-dimensional imaging with multiplex coherent anti-Stokes Raman scattering microscopy," Opt. Lett. **27**(13), 1093–1095 (2002).
43. S. H. Parekh, Y. J. Lee, K. A. Aamer, and M. T. Cicerone, "Label-free cellular imaging by broadband coherent anti-Stokes Raman scattering microscopy," Biophys. J. **99**(8), 2695–2704 (2010).
44. T. Baldacchini and R. Zadoyan, "*In situ* and real time monitoring of two-photon polymerization using broadband coherent anti-Stokes Raman scattering microscopy," Opt. Express **18**(18), 19219–19231 (2010).
45. R. A. Andersen, *Algal Culturing Techniques* (Academic–Elsevier, San Diego, CA, 2005).
46. Y. Y. Huang, C. M. Beal, W. W. Cai, R. S. Ruoff, and E. M. Terentjev, "Micro-Raman spectroscopy of algae: composition analysis and fluorescence background behavior," Biotechnol. Bioeng. **105**(5), 889–898 (2010).
47. T. G. Tornabene, G. Holzer, S. Lien, and N. Burris, "Lipid composition of the nitrogen starved green alga Neochloris oleoabundans," Enzyme Microb. Technol. **5**(6), 435–440 (1983).
48. G. H. Krause and E. Weis, "Chlorophyll fluorescence and photosynthesis: the basics," Annu. Rev. Plant Physiol. Plant Mol. Biol. **42**(1), 313–349 (1991).
49. N. E. Holt, J. T. M. Kennis, and G. R. Fleming, "Femtosecond fluorescence upconversion studies of light harvesting by β-carotene in oxygenic photosynthetic core proteins," J. Phys. Chem. B **108**(49), 19029–19035 (2004).

1. Introduction

Recently, microalgae have been extensively researched for their potential as feedstocks for renewable biofuel production [1–3]. Unicellular microalgae have the capability to harness sunlight and CO_2 to produce energy-rich chemical compounds, such as lipids and carbohydrates, which can be converted into fuels [1,3,4]. However, lipids in microalgae require efficient characterization techniques to investigate the metabolic pathways and the environmental factors influencing their accumulation. The model green alga *Coccomyxa* accumulates significant amounts of triacylglycerols (TAGs) under nitrogen depletion (N-depletion) [5]. Due to its capability of detecting vibrational information of a system, Raman scattering spectroscopy and microscopy are suitable for characterization of microalgae. Rapid composition analysis using Raman spectroscopy can greatly facilitate the selection of suitable algal strains and their associated growing conditions for different applications, ranging from biofuels to nutritional supplements [6–9].

Since Raman scattering signals are very weak (typical photon conversion efficiencies for Raman are lower than 1 in 10^7), microscopy based on Raman scattering requires high laser average powers and long integration times ranging from 100 ms to 1 s per pixel [10]. This drawback has severely blocked the applications of Raman microscopy to the study of living systems. Coherent anti-Stokes Raman scattering (CARS) signals, based on the mixing of four waves in a nonlinear optical process, are much stronger than Raman signals and thus more suited for microscopy applications that require real-time imaging [11]. CARS was first reported in 1965 by Maker and Terhune [12] as a spectroscopy method for chemical analysis. CARS involves the interaction of four waves designated as pump (p), Stokes (s), probe (p'), and anti-Stokes (CARS), where pump and probe are usually fixed to the same frequency ($\omega_\rho = \omega_{\rho'}$). When the beat frequency between the pump and the Stokes beams matches a Raman active vibrational mode Ω_R of the molecules or lattice in the sample, a strong and coherent anti-Stokes signal is generated, greatly promoting sensitivity with chemical selectivity. A drawback of CARS in respect to spontaneous Raman scattering is that signals generated by

#175376 - $15.00 USD Received 4 Sep 2012; revised 13 Oct 2012; accepted 15 Oct 2012; published 18 Oct 2012

CARS are dispersive due to the presence of a nonresonant signal. The presence of the latter mixed with the resonant signal makes CARS data interpretation more challenging than data obtained with spontaneous Raman scattering [13].

CARS [14,15] is much more efficient than spontaneous Raman spectroscopy [16–18], enabling faster, more sensitive analyses with less photo exposure. CARS circumvents the need for extrinsic labels, allowing observation of dynamic phenomena for which tags are not available. CARS also enables detection in the presence of one-photon fluorescence, 3-D sectioning, and penetration to a depth of ~0.4 mm while minimizing photo damage [19–21]. CARS microscopy has been utilized to image living cells with signals generated from different vibrational modes, such as the amide I vibration from protein, OH stretching from water, phosphate stretching from DNA, and the CH group of stretching from lipids [11,22–25]. There are also many other examples, such as single phospholipid bilayer visualization [26], the trafficking and growth of lipid droplets [27], intracellular water diffusion, and biomedical imaging of tissues *in vivo* [21]. CARS has been used also for two-photon polymerization [28–30] and carbon nanotube [31] characterization. In this study, we employ broadband CARS, which was first proposed by Akhmanov *et al.* [32].

Recently, a newly developed label-free chemical imaging technique called stimulated Raman scattering (SRS) microscopy has been used for a variety of samples, including algae samples [33]. This technique overcomes the speed limitation of confocal Raman microscopy while avoiding the nonresonant background problem of CARS microscopy [34–38].

CARS spectroscopy is accomplished by collecting the scattering signals with a spectrometer. When using narrow bandwidth pump and Stokes sources [39,40], the wavelength of the Stokes or pump beam is scanned to get a CARS spectrum (intensity versus Raman shift). This process is time consuming and makes it difficult to follow dynamics in a biological structure. However, a single-shot CARS spectrum can be achieved with a broad Stokes beam and a narrow pump beam. The broad Stokes beam in collinear alignment with a narrow pump beam will excite a wide range of Raman transitions [13]. It is desirable to have a Stokes beam with a broad spectrum for fast spectrum generation. A potential method is to employ a supercontinuum (SC) source for the generation of laser pulses with 4000-cm^{-1} bandwidth [41], which is not possible (too wide) for femtosecond (fs) pulses. Significant advances in the development and fabrication of photonic crystal fibers (PCF) facilitated the use of PCF as a stable, reliable solution for supercontinuum generation, since an input of tens of mW from an fs oscillator is sufficient. Therefore, broadband CARS (B-CARS) [39,42,43] that uses an fs pump beam (ω_p) and a super-continuum Stokes beam (ω_s) for fast acquisition of CARS spectra was employed in this study. The Stokes beam has broad spectral bands that allow simultaneous stimulation and detection of Raman shifts over a wide range.

In this study, we investigated both spontaneous Raman scattering and CARS spectroscopy and microscopy to detect different components in microalgae. The model green alga *Coccomyxa* accumulates significant amounts of TAGs under nitrogen depletion (N-depletion). Therefore, *Coccomyxa subellipsoidea* C169 algae were used for this study to investigate the lipid growth for biofuel research. Raman spectra of control and N-depleted microalgae were compared to distinguish changes in algae under the N-depletion condition, since high lipid (energy-rich compound) production in microalgae is desired for biofuel generation. CARS spectra were also measured to compare with Raman spectra. CARS microscopy imaging was compared to Raman imaging to show its advantages on acquisition speed and spatial resolution.

2. System Description

2.1 CARS spectroscopy and microscopy system

In this study, broadband CARS microscopy based on a photonic crystal fiber light source has been used to measure microalgal cells. A wavelength extension unit (WEU) from Newport

#175376 - $15.00 USD Received 4 Sep 2012; revised 13 Oct 2012; accepted 15 Oct 2012; published 18 Oct 2012

was used in this study [44]. Although a full description of the WEU can be found elsewhere [44], a short account on the most critical parts of this unit is described here. The pump pulses have a narrow bandwidth and define the spectral resolution. The Stokes pulses are spectrally broad ranging from below 700 nm to over 1100 nm [44]. The pump and Stokes pulses excite multiple Raman transitions within the bandwidth of the Stokes pulses. Vibrationally excited states are probed with a third spectrally narrow probe pulse, usually the same as the pump pulse. In a single shot, the entire CARS spectrum of the excited states is generated. Both the pump and Stokes beams are provided by a single fs laser (MaiTai DeepSee HP, SpectraPhysics) in conjunction with a supercontinuum generator (SCG-800-CARS, Newport) [44], which is optimized for performing broadband CARS microscopy. The SCG ensures that broadband anti-Stokes spectra can be obtained without tuning the laser wavelength. As shown in Fig. 1, the laser was isolated from the rest of the setup by means of a Faraday isolator (FI). The laser output was divided into two beams to form the pump and Stokes beams. A 50/50 ultrafast beam splitter designed for S-polarization was used. Rotation of the input polarization with a 1/2 wave plate continuously varied the splitting ratio between 20% and 50%. Each arm of the setup had a variable attenuator, allowing independent control of intensity and polarization. The Stokes beam was formed by filtering through a long-pass filter LP (RG750, Newport) after the collimating objective, and then passed an 808 nm razor edge long-pass filter (RELP) (LP02-808RU-25, Semrock). A second long-pass filter LP (RG750, Newport) provided additional filtering of the visible light. The Stokes beam was then routed into the back aperture of the focusing objective and focused into the sample. The other 800 nm beam passed through an attenuator and was guided to a delay line. The bandpass filter (LL01-808-25, Semrock) narrowed the spectrum of the 800 nm beam down to 3 nm to form the pump beam. The filter was mounted on a rotation stage, and the angle of incidence was adjusted to

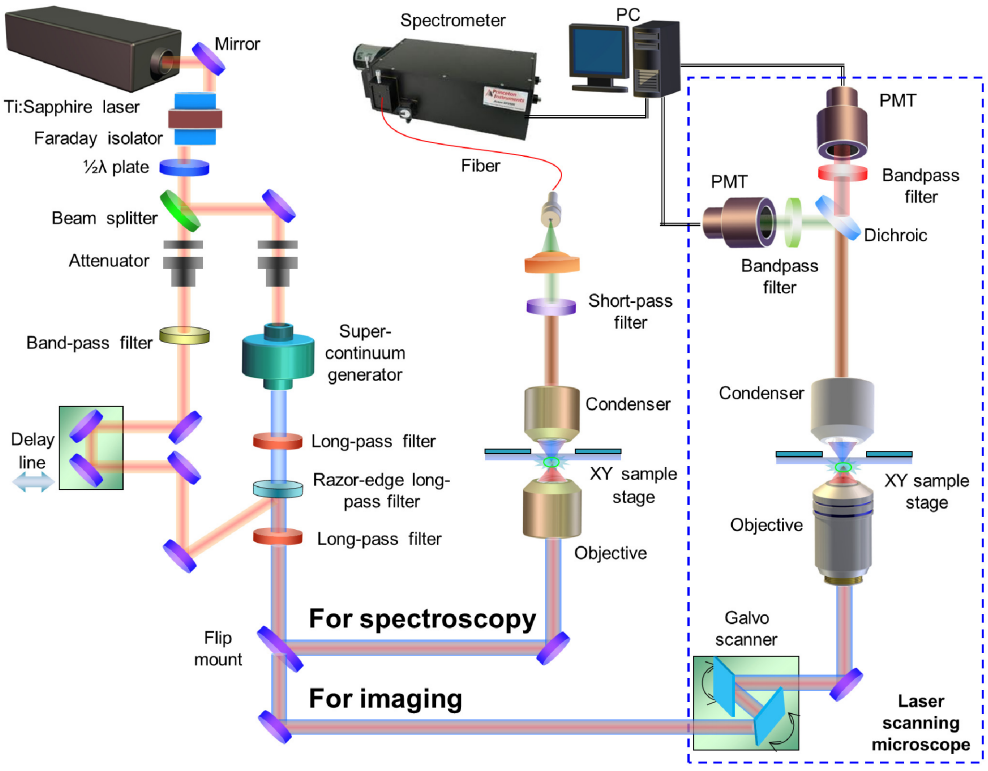

Fig. 1. Schematic setup of the broadband forward CARS spectroscopy and microscopy system.

#175376 - $15.00 USD Received 4 Sep 2012; revised 13 Oct 2012; accepted 15 Oct 2012; published 18 Oct 2012

shift the center of the band to 800 nm. The pump beam recombined with the Stokes beam after reflecting from an 808 nm RELP long-pass filter (LP02-808RU-25, Semrock). The collinear pump and Stokes beams were recombined after a razor-edge long-pass filter and then projected onto a sample through a 40× objective (M-40× , Newport) lens to generate CARS signals with a 10× condenser lens (M-10×, Newport). The combination of a short-pass filter (Edmund Optics, NT 47-588) positioned after the sample transmits wavelengths shorter than 780 nm. The flip mirror mount (FM) was used to direct the collimated anti-Stokes beam into a spectrometer or photomultiplier (PMT) in a laser scanning microscope (LSM). A spectrometer (SP2300i, Princeton Instruments) was used to acquire the CARS spectra.

Beside acquisition of CARS spectra, a laser scanning microscope (BX61WI, Olympus) was used for CARS microscopy. The galvo scanner in the LSM was used to scan the collinear pumping and Stokes beams on the sample. There are four PMT channels in the LSM that were used to detect the CARS signal from the laser spot with their positions registered in the PC. The software used was FV1000 (Olympus), which comes with the LSM. The bandpass filter used for CARS was Semrock FF01-647/57, $T_{avg} > 92\%$ 618.5-675.6 nm, center $\lambda = 647$ nm, and bandwidth 57 nm. The autofluorescence filter used was Olympus BA420-460 (420-460 nm). The objective employed was PLAN 25× objective with water immersion, a numerical aperture (NA) of 1.05, and a working distance (WD) of 2 mm. The pump and Stokes beam provided for CARS imaging was the same as the CARS spectroscopy from a Mai Tai DeepSee HP DS femtosecond laser in conjugation with an SCG. The substrate used for measuring algal cells was transparent glass slides with coverslips on top. The bandpass filter used for CARS imaging was 650 nm with a full width at half maximum (FWHM) of 40 nm, while the bandpass filter used for autofluorescence was at 450 nm with an FWHM of 10 nm. The software used was Olympus FV1000 for imaging generation and ImageJ for 3-D image generation.

2.3 Raman spectroscopy

The Raman system used here was a Renishaw inVia dispersive micro-Raman spectrometer with 514-nm Ar^+ laser excitation. The laser power used was 5 mW with an exposure time of 10 sec for Raman spectroscopy and ~3 hr for Raman imaging with 1 μm step size and a scanning speed of 5 sec per step. The substrate used was a 100 nm gold-coated silicon wafer (Platypus Technologies, LLC). Raman image generation was realized using software from Renishaw, named WiRE 3.2; and Origin 7.5 was used for spectral graph generation.

2.4 Algal culturing

Algal culturing using *Coccomyxa subellipsoidea* (*Coccomyxa* sp.) C169 was carried out in this study. Cultures used for inoculum were maintained on agar plates containing Bold's basal medium (BBM) [33] with double the normal nitrate concentration and 100 mg L^{-1} carbenicillin (Fisher Scientific, Pittsburg, PA). Liquid batch cultures were first established in BBM from picked colonies and allowed to reach the early stationary phase at 25°C and 120 rpm in a lighted shaking incubator (Innova 43, New Brunswick Scientific, Enfield, CT). Abiotic stress was induced through nitrogen limitation by centrifugation, removal of media containing nitrate, and suspension of the algal pellet in sterile nitrogen-free BBM at an approximate concentration of 5 million cells per milliliter [45].

3. Results and Discussion

3.1 Spontaneous Raman scattering spectroscopy and microscopy of microalgae

The algal cell used was *Coccomyxa* sp. (strain C169), grown under nitrogen-depleted conditions to promote triglyceride (TAG) (lipid) accumulation. Lipid has many Raman peaks, which can be seen in Table 1. When the algal cells were grown in the control environment, there were very strong carotenoid Raman peaks at 1004, 1160, and 1520 cm^{-1}. However,

#175376 - $15.00 USD Received 4 Sep 2012; revised 13 Oct 2012; accepted 15 Oct 2012; published 18 Oct 2012

when the algal cells were prepared in an N-depleted environment, we observed significant Raman peaks at 1440, 1650, and 2840–2950 cm^{-1} (as indicated in Fig. 2), which can be assigned to lipid signals. Figure 2 shows the Raman spectra of control (blue) and N-depleted (red) algal cells. The most prominent difference is the strong lipid peaks for the cells grown under the N-depletion environment. Growth conditions can have a significant effect on the composition of algal cultures. It is known that algal cells increase TAG production during nitrogen starvation [46]. With additional data processing algorithms and the development of standardized calibrations for the spectral analysis, Raman spectroscopy has the potential to provide a rapid composition analysis tool for the quantification of TAG content or other components, such as carotenoids. This would be extremely useful to the growing industry striving to produce fuels and chemicals from algae.

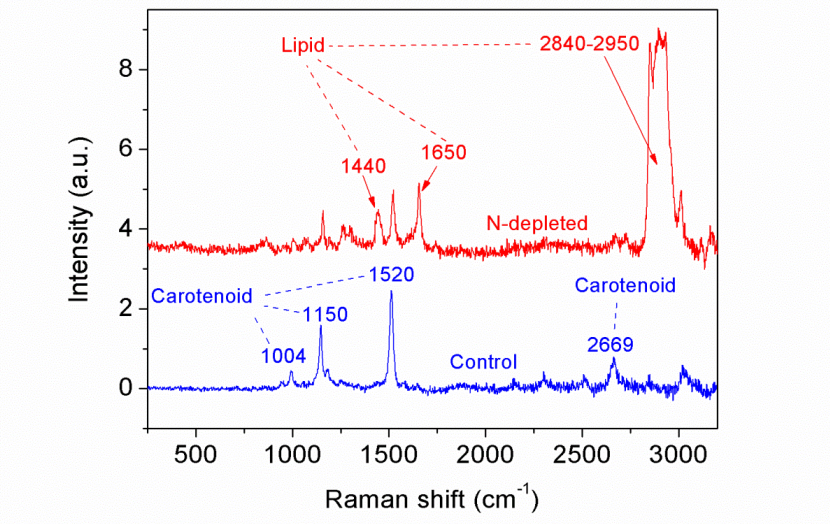

Fig. 2. Spontaneous Raman spectroscopy using 514.5-nm excitation. Top (red solid) shows the Raman spectrum of a nitrogen-depleted microalgal cell (*Coccomyxa* sp. c-169). Bottom (blue solid) shows the Raman spectrum of a control microalgal cell.

Table 1. Raman peak assignment of the Raman spectra of microalgae

Raman peaks (cm^{-1})	Components	Peak assignment
1004	Carotenoid	Carotene C-H bend
1056,1116	Lipid	Alkyl C-C trans and gauche stretches
1075	Lipid	Alkyl C-C gauche stretches
1150	Carotenoid	Carotene C-H stretches
1260	Lipid	Alkyl = C-H cis stretches
1300	Lipid	Alkyl C-H_2 twist
1440	Lipid	Alkyl C-H_2 bend
1520–1538	Carotenoid	Carotene C = C stretches
1650	Lipid	Alkyl C = C stretches
2800-3000	Lipid, carbohydrate	CH_2 symmetric and asymmetric stretches
3023	Lipid	Alkyl = C-H stretches

As shown in Fig. 3, optical microscopy images of control cells (a) and N-depleted cells (b) on a gold surface were taken, which shows the live algal cells in solution. Comparing (a) and (b), we find that there are more small droplets inside each N-depleted algal cell. There are more cells in Fig. 3 (b) simply because the cell concentration of N-depleted cells is higher than control cells. The Raman maps shown in Fig. 4 provide a qualitative assessment of the relative composition of algae via Stokes Raman scattering. Figure 4(b) confirms that a significant portion of the cell is composed of lipids when the cells are grown in an environment lacking nitrogen (N-depletion). The spectral imaging is based on the signal

#175376 - $15.00 USD Received 4 Sep 2012; revised 13 Oct 2012; accepted 15 Oct 2012; published 18 Oct 2012

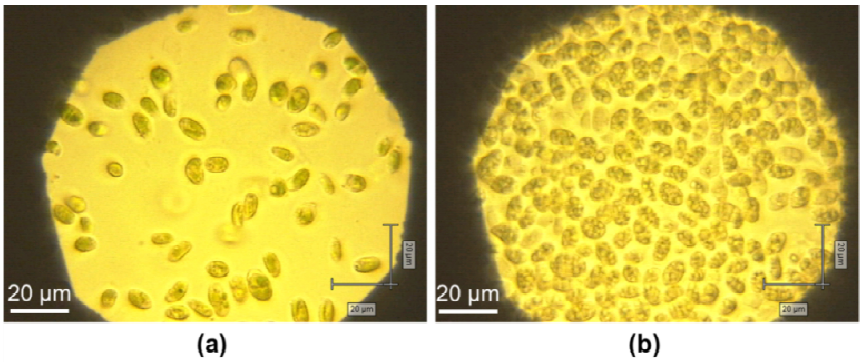

Fig. 3. Optical microscopy images of control cells (a) and N-depleted cells (b) on gold surface.

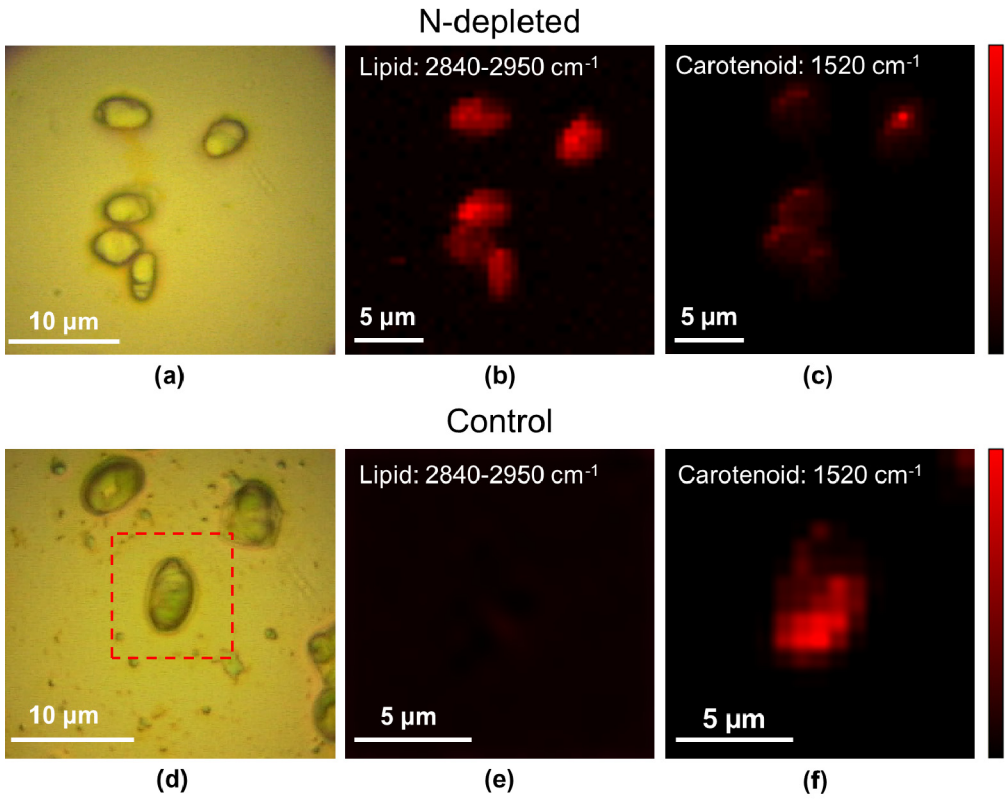

Fig. 4. Spontaneous Raman spectral imaging of dried microalgae. (a) Optical image of dried N-depleted microalgae on a gold surface. (b) Raman image of (a) at 2840-2950 cm^{-1} TAG CH_2 stretching modes. (c) Raman image of (a) at 1520 cm^{-1} (or 1482-1555 cm^{-1}) carotenoid C = C stretching mode. (d) Optical image of dried control microalgae on a gold surface. (e) Raman image of (d) at 2840-2950 cm^{-1} TAG CH_2 stretching modes. (f) Raman image of (d) at 1520 cm^{-1} (or 1482-1555 cm^{-1}) carotenoid C = C stretching mode. LUTs are shown after (c) and (f).

intensity between 2840 and 2950 cm^{-1}, with the baseline subtracted. Applying nitrogen-starvation for a longer duration has been shown to yield even greater lipid content in algae [1,47].

The algal cells in Fig. 4 are all dried out due to long exposure during Raman imaging (~3 hr). An optical micrograph of *Coccomyxa* sp. C169 N-depleted algal cells is shown in Fig. 4(a). Figures 4(b) and 4(c) are spectral composition maps that were constructed from acquired

#175376 - $15.00 USD Received 4 Sep 2012; revised 13 Oct 2012; accepted 15 Oct 2012; published 18 Oct 2012

spectra at each pixel point. The signal intensity within the desired wavenumber regions (1505-1535 cm^{-1} for carotenoid and 2840-2950 cm^{-1} for TAG) were measured for every spectra, and the map was created such that locations with high intensity were denoted in bright red and those with low intensity were denoted in black. Figure 4 demonstrates the Raman imaging of single algal cells with and without N-depletion, respectively. N-depleted algae (Figs. 4(a)–4(c)) mainly contain TAG droplets with little carotenoid, while control algae (Figs. 4(d)–4(e)) contain much more carotenoid and little signal from lipid. Lookup tables (LUTs) are shown in Figs. 4(c) and 4(f).

One limitation of spontaneous Raman spectroscopy is that fluorescence can overwhelm the component specific peaks in some cases. Therefore, Raman spectroscopy with near infrared excitation wavelengths (e.g., 785 nm) and coherent anti-Stokes Raman spectroscopy are much more suitable for algae imaging. However, the actual resolving power of spontaneous Raman spectroscopy is limited to about 1 μm due to the diffraction of light, which may cause the detection of components with small dimension less possible. For instance, some amount of TAG may present in control and starved cultures of *Coccomyxa*. Therefore, CARS imaging was used for measurement of algae cells for improved sensitivity and scanning speed.

3.2 Coherent anti-Stokes Raman spectroscopy and microscopy of microalgae

CARS imaging of algal cells using a laser scanning microscope system (Fig. 5(a)) was carried out to study the *Coccomyxa* algal cells. Higher spatial resolution can be achieved using this system (<500 nm). Figure 5 (a) is a bright field transmission optical microscopic image of N-depleted cells. The small black dots in each cell are TAG droplets. A significant difference between the control (Fig. 5(b)) and N-depleted cells (Fig. 5(c)) is the existence of much more lipid droplets in the N-depleted cells. The brighter points in the images represent a higher lipid signal (2800-3000 cm^{-1}). The Figs. 5(b) and 5(c) are 2048 × 2048 pixels with a sampling speed of 2 μs per pixel.

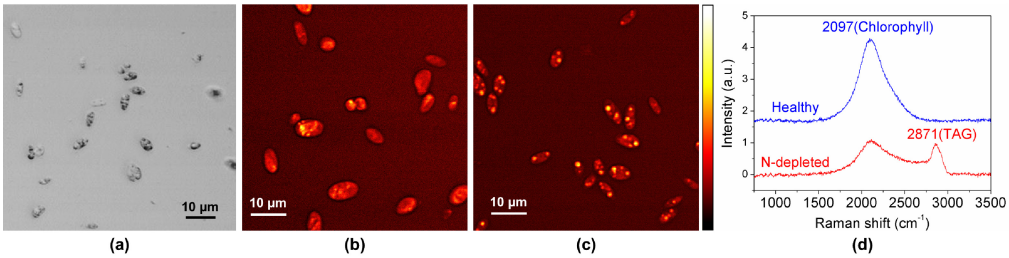

Fig. 5. (a) Transmission optical microscopy image of N-depleted algal cells, in which the black dots are TAG droplets. (b) CARS image of control microalgae. (c) CARS image of N-depleted microalgae. (d) CARS spectra of control (blue) and N-depleted (red) microalgae. An LUT table is shown after (c).

CARS spectra of the algal cells were also acquired using the B-CARS spectroscopy system. In Fig. 5(d), CARS spectra of control (blue) and N-depleted live algal cells are presented. Besides the lipid peak at 2871 cm^{-1}, there is another broad peak at 2097 cm^{-1} (corresponding to a wavelength of 685 nm), which is due to the two-photon excited fluorescence of chlorophyll in the algae, which has a wavelength of 680 nm [48], in the algal cells. When the cells were prepared in a control environment, the chlorophyll part was greater than in the N-depleted cells, which can be seen directly from the solutions with algae cells (more greenish color in the control cell solution). A drawback of CARS imaging is that there is an overlap between the two-photon excited fluorescence of chlorophyll and the CARS signal of lipid, as shown in Fig. 5(d).

#175376 - $15.00 USD Received 4 Sep 2012; revised 13 Oct 2012; accepted 15 Oct 2012; published 18 Oct 2012

In Fig. 6, algae cells were dried out before CARS imaging. The figures are 1024 × 1024 pixels with a sampling speed of 20 µm. The two images in Fig. 6 were taken at exactly the same imaging parameters, such as laser power. The cells with N-depletion have a much higher intensity of lipid (brighter) (Fig. 6(b)); however, the image of the control cells (Fig. 6(a)) is very dark, indicating much less lipid containment. The contrast in Fig. 6(a) came from two sources. One was the interference from the two-photon fluorescence of chlorophyll in the algae, while the other was possibly from the membrane lipid of the algal cells.

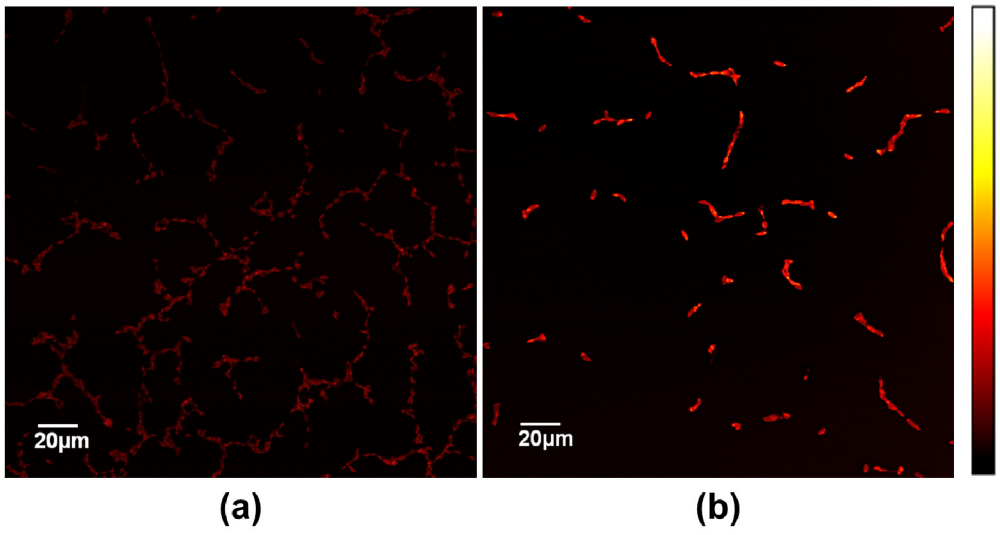

Fig. 6. CARS microcopy of dried algal cells. (a) Control algal cells. (b) N-depleted algal cells. An LUT is shown after (b).

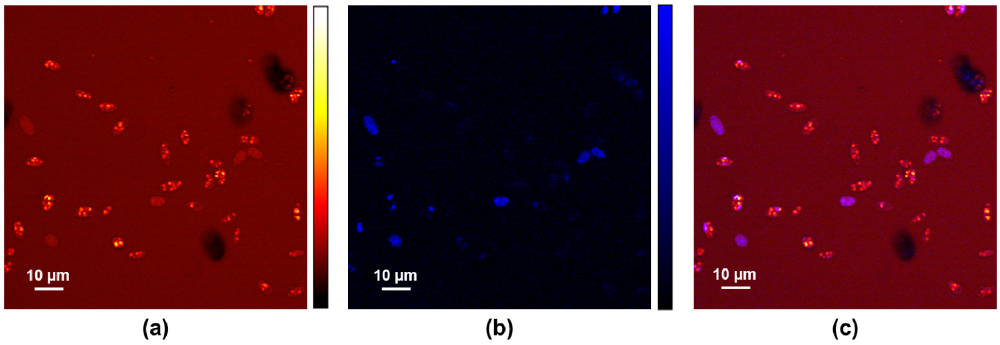

Fig. 7. (a) CARS image (618.5-675.5 nm) of partially N-depleted microalgae. (b) Autofluorescence (420-460 nm) acquired the same time as the CARS image. (c) Composite image of CARS (a) and autofluorescence (b). LUTs are shown after (a) and (b).

Figure 7(a) is a CARS image of lipids in live algal cells grown in an N-depleted environment. The figure was acquired 640 × 640 pixels with a sampling speed of 4 µs per pixel. Each of the cells has many TAG droplets with a very high lipid signal (very bright points), indicating a positive relationship between lipid increase and N-depletion treatment. In Fig. 7(b), we used a bandpass filter centered at 450 nm with an FWHM of 10 nm for autofluorescence acquisition. The autofluorescence signal was very weak compared to the CARS signal. Therefore, the contrast of Fig. 7(b) was increased to give a better view of this image. The autofluorescence parts exist mostly in the outer area of the cells, which is due to

#175376 - $15.00 USD Received 4 Sep 2012; revised 13 Oct 2012; accepted 15 Oct 2012; published 18 Oct 2012

the two-photon excited fluorescence of β-carotenoid components of the cells [49]. Figure 7(c) is a composite image of Figs. 7(a) and 7(b).

Algal cells in Fig. 8 were prepared much longer in a nitrogen-depleted environment. The figures in Fig. 8 had 1600 × 1600 pixels with a sampling speed of 20 µs per pixel. Each of the algal cells has many lipid droplets inside of it. The intensity of the carotenoid fluorescence (420-460 nm) is much lower compared to that in Fig. 7, due to the fact that there is much less carotenoid in these cells compared to those in Fig. 7. The lipid droplet in Fig. 7(a) is less bright than that in Figs. 5(c) and 8(a), due to the fact that the sample measured in Fig. 7 was grown in N-depleted environment for a shorter time than that in Figs. 5(c) and 8(a). Therefore, their fluorescence in Fig. 7(b) is also much stronger than that in Fig. 8(b). This is mainly due to the growth time of the microalgal cells in the N-depleted condition.

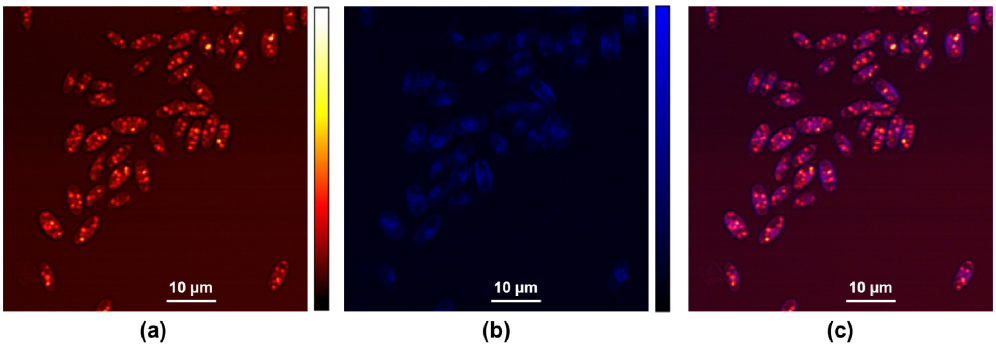

Fig. 8. (a) CARS image (618.5-675.5 nm) of totally N-depleted microalgae. (b) Autofluorescence (420-460 nm) acquired at the same time as the CARS image. (c) Composite image of CARS (a) and autofluorescence (b). LUTs are shown after (a) and (b).

4. Conclusion

A broadband CARS system was built for CARS spectroscopy and microscopy. A pair of objective lenses was used for CARS spectroscopy, while a laser-scanning-microscope-based CARS microscopy system was realized and used for CARS imaging of algal cells, with a specific focus on triglyceride accumulation. The CARS spectroscopy and imaging were compared to spontaneous Raman spectroscopy and imaging. Microalgal cells, with or without nitrogen depletion, were measured. CARS spectra of microalgae were successfully taken using the CARS system. The Raman spectra, from a commercial Raman spectrometer, were taken from microalgal cells with or without N-depletion, for comparison with the CARS spectra. The spectral resolution of Raman spectroscopy is much better than the B-CARS spectroscopy. Although the Raman imaging capability is not as strong from both the speed and spatial resolution perspectives for the laser-scanning-microscope-based CARS system, the CARS imaging of microalgae has a drawback of signal overlapping with two-photon excited fluorescence. In future research, more study will be done to improve the CARS microscopy with reduced nonresonant background, and the microalgae growth in N-depletion environment will be monitored in real-time and in *vivo* to further investigate metabolic pathway of lipids.

Acknowledgments

This research work was financially supported by the National Science Foundation MRI program (CMMI 1126208), Office of Naval Research (N000140910943), and UNL Life Sciences Competitive Grants Program.

#175376 - $15.00 USD Received 4 Sep 2012; revised 13 Oct 2012; accepted 15 Oct 2012; published 18 Oct 2012